Available online at www.sciencedirect.com
ScienceDirect
Cement & Concrete Composites 29 (2007) 626–636
Cement & Concrete Composites
www.elsevier.com/locate/cemconcomp

Influence of paste volume on shrinkage cracking and fracture properties of self-compacting concrete

E. Rozière [a], S. Granger [a], Ph. Turcry [b], A. Loukili [a,*]

[a] Civil Engineering and Mechanics Research Institute (GeM), UMR CNRS 6183, Ecole Centrale de Nantes, 1 rue de la Noë, BP 92101, 44321 Nantes Cedex 3, France
[b] LEPTAB, University of La Rochelle, Avenue Michel Crepeau, 17042 Cedex 01, France

Received 11 July 2006; received in revised form 16 March 2007; accepted 26 March 2007
Available online 18 April 2007

Abstract

Self-compacting concrete (SCC) mixtures are usually designed with higher volumes of paste than vibrated concrete mixtures. The results reported in this paper come from a study of nine SCC concrete mixtures. Volume of paste was varied between 291 and 457 l/m^3. One of the mixtures had already been used in a large scale test, and the others were designed by varying several parameters of the reference concrete mixture. Mechanical properties, shrinkage, fracture parameters and fracture process zone (FPZ) size were measured. Fracture behavior was characterized by means of three-point bending tests and acoustic emission analysis. From the experimental results, increasing the volume of paste has a restricted effect on strength, unless water content varies. Strength, elastic modulus and fracture resistance slightly decrease with an increase in paste content. Volume of paste causes an increase in shrinkage and cracking due to shrinkage. Fracture and acoustic emission analysis show that increasing the volume of paste tends to make SCC more brittle.

Keywords: Self-compacting concrete; Volume of paste; Shrinkage; Mechanical properties; Cracking; Fracture; Acoustic emission

1. Introduction

Self-compacting concrete (SCC) represents a major evolution in the building industry. Its positive features result from the elimination of mechanical compaction. Compared to ordinary vibrated concrete, SCC offers many advantages in terms of both technology and worker health [1]. For instance, SCC can be used to solve special casting problems (congested reinforcement, slender structures, etc.). One interesting benefit is the enhancement of the working conditions in building sites, especially the suppression of health problems associated with the vibration task.

To promote the use of SCC, a French project called PN B@P began in 2000, supported by the building industry and research laboratories. Studies were performed to understand better the behavior of SCC and particularly shrinkage cracking. Questions about cracking susceptibility of SCC are often raised, because SCC is designed with a higher volume of paste than ordinary concrete [2]. The volume of paste of a concrete mixture is usually defined as the sum of the volumes of cement, water, mineral addition and chemical admixtures. Increasing the volume of paste improves flowability but it may have unexpected effects on mechanical properties and time-dependent deformations. For example, drying shrinkage is known to increase with the volume of paste [3].

This paper compiles the results of an experimental investigation on the effects of volume of paste on properties involved in the mechanism of shrinkage cracking. Three series of concrete mixtures were tested. In the first series, the volume of paste of a reference mixture was varied with constant proportions. In the second and third series, the volume of paste of the reference mixture was varied by changing, respectively, the water content or the mineral

* Corresponding author. Tel.: +33 240 37 1667; fax: +33 240 37 2535.
E-mail address: ahmed.loukili@ec-nantes.fr (A. Loukili).

0958-9465/$ - see front matter © 2007 Published by Elsevier Ltd.
doi:10.1016/j.cemconcomp.2007.03.010

addition content. The characterization of the mixtures included mechanical tests, free shrinkage measurements and restrained shrinkage tests (ring tests) to assess the risk of shrinkage cracking. Moreover, bending tests were performed on some mixtures of the first series to study the effect of the volume of paste on the fracture behavior. The experimental data reported in this paper could be useful for optimizing SCC mixtures and for the development and validation of models.

2. Experimental program

2.1. Materials

A rolled 3/8 mm gravel (G) and well-graded 0/4 mm sea sand (S) were used in all the mixtures tested in our study. The sand fines content (<80 μm) was lower than 1%. A CEM I 52.5 cement (C) and limestone filler (LF) were used. Their compositions and properties are given in Table 1. The deflocculation of fine particles was ensured thanks to a polycarbolaxate type superplasticizer (Sp). A viscosity enhancing agent (VEA) was also used to increase the segregation resistance. The mixtures were made with tap water. The efficient water content, i.e. the total water content minus the water volume absorbed by aggregate, is denoted W_{eff} in the followings.

2.2. Mixtures

An SCC mixture designed with the previously described contents was used during the PN B@P in a large scale test in Guerville, France. This concrete mixture, called Ref, is taken as a reference of the three series of mixtures described hereafter. All the mixtures have the same G/S and VEA/W_{eff} ratios.

- *Series 1* (Table 2). The volume of paste of the Ref mixture, denoted V_P, is reduced or increased within a range of −30% to +10 %, in order to obtain four other mixtures. The volume of paste is changed but its composition remains the same, i.e. the W_{eff}/C and LF/C ratios are all kept constant.
- *Series 2* (Table 3). The efficient water content (W_{eff}) is increased by 20 and 40 l by reducing the aggregate content. The LF/C ratio is kept constant.

Table 1
Properties of cement and limestone filler

	CEM I 52.5	Limestone filler (LF)
Clinker (%)	100	–
$CaCO_3$ (%)	–	98
C_3S (%)	60	–
C_2S (%)	20	–
C_3A (%)	5	–
C_4AF (%)	10	–
Blaine (m^2/kg)	405	397

- *Series 3* (Table 3). The limestone filler content (LF) is increased or decreased by 44% by changing the aggregate content. The W_{eff}/C ratio is kept constant. It should be noted that 44% of the limestone filler mass corresponds to 10% of the volume of paste of the Ref mixture.

The superplasticizer content is adjusted to produce slump flow between 60 and 80 cm, typical values for SCC. It is assumed that variations in superplasticizer content have low effect on hardened concrete properties.

2.3. Experimental procedures

2.3.1. Mixing procedure, fresh state tests and curing

The mixing procedure is the following. Solid contents, i.e. gravel, sand, cement and limestone filler are first introduced and mixed 30 s. Then, water and VEA are progressively added. After 30 s, the superplasticizer is poured and the constituents are mixed for 3 min.

After mixing, slump flow and flow time, i.e. the time to reach the final slump flow, are measured. The segregation resistance is controlled using the sieve test, also called screen stability test [4]. This test consists in pouring about 4.8 kg of fresh concrete onto a 5 mm sieve. After 2 min, the weight of the paste which passes through the sieve (laitance) is measured. If the percentage of laitance does not exceed 15% of the sample, the stability of the tested mixture is supposed to be satisfactory.

Fifty liters of each mixture were made and cast into eighteen 11×22 cm cylindrical molds, three $7 \times 7 \times 28$ cm prismatic molds and one ring. Air content was assessed through measurements of density on the cylindrical samples at fresh state (see Tables 2 and 3). Before testing, the specimens were stored in a room at 20 °C and 95% relative humidity (RH).

2.3.2. Mechanical properties

Mechanical properties (compressive strength, tensile strength, elastic modulus) were measured on 11×22 cm cylinders at 2, 7 and 28 days. Tensile strength was assessed through splitting tests. The elastic modulus was determined with a *Grindosonic* apparatus. This device gives the frequency of a vibration created by a slight shock on the sample and the elastic modulus is calculated from this frequency with the Spinner and Teft Model [5]. All tests were carried on three samples and the given results are average values.

2.3.3. Shrinkage tests

From the age of one day, total shrinkage, i.e. shrinkage due to drying and cement hydration, was measured on $7 \times 7 \times 28$ cm prisms using LVDT sensors, in a room at 20 ± 2°C and 50 ± 5% RH. Autogenous shrinkage was measured in the same way, on prisms sealed with a double layer of adhesive aluminum. In parallel, the mass of

Table 2
Compositions and properties of the Series 1 mixtures

	Series 1 (kg/m^3)				
	$V_p - 30\%$	$V_p - 20\%$	$V_p - 10\%$	V_p (Ref)	$V_p + 10\%$
Gravel	964	906	848	790	732
Sand	817	768	719	670	621
Cement	256	292	329	365	402
Limestone filler	179	204	230	255	281
W_{eff}	139	159	179	199	219
VEA	0.46	0.53	0.59	0.66	0.73
Sp	6.24	5.44	5.50	5.20	4.92
Vol. of paste (l)	291	332	374	415	457
V_{LF}/V_C	0.8	0.8	0.8	0.8	0.8
W_{eff}/C	0.54	0.54	0.54	0.54	0.54
W_{eff}/(C + LF)	0.32	0.32	0.32	0.32	0.32
Slump flow (mm)	680	760	800	800	800
Flow time (s)	25	14	7	8	9
Sieve test (%)	0.6	4.9	8.5	15.6	11.1
Density	2.32	2.33	2.31	2.28	2.27
Air content (%)	5.2	3.4	3.4	3.4	2.8
fc (MPa)	47.1	46.7	41.5	44.8	41.7
ft (MPa)	4.7	4.5	4.3	4.1	4.1
E-modulus (GPa)	38.7	37	34.8	34	32.8
Age of cracking (d)	>420	>90[a]	>210	120	71
Total shrinkage at 120 d (μm/m)	300	330	370	420	450

[a] The ring test on $V_p - 20\%$ mixture was stopped at 90 days.

Table 3
Compositions and properties of the Series 2 and 3 mixtures

	V_p (Ref)	Series 2 (kg/m^3)		Series 3 (kg/m^3)	
		W_{eff} + 20 l	W_{eff} + 40 l	LF − 44%	LF + 44%
Gravel	790	762	734	848	732
Sand	670	646	623	719	621
Cement	365	365	365	365	365
Limestone filler	255	255	255	143	367
W_{eff}	199	219	239	199	199
VEA	0.66	0.73	0.79	0.66	0.66
Sp	5.20	3.30	2.80	5.00	6.20
Vol. of paste (l)	415	433 (V_p + 4.3%)	452 (V_p + 8.9%)	372 (V_p − 10%)	456 (V_p + 10%)
V_{LF}/V_C	0.8	0.80	0.80	0.46	1.14
W_{eff}/C	0.54	0.60	0.65	0.54	0.54
W_{eff}/(C + LF)	0.32	0.35	0.38	0.39	0.27
Slump flow (mm)	800	700	710	720	760
Flow time (s)	8	6	1	6	7
Sieve test (%)	15.6	2.5	2.7	6.0	7.9
Density	2.28	2.27	2.25	2.28	2.28
Air content (%)	3.4	2.1	1.7	2.8	3.3
fc (MPa)	44.8	34	33	38.8	42.8
ft (MPa)	4.1	2.9	2.8	3.6	4.3
E modulus (GPa)	34	32.4	32.4	33.4	33.6
Age of cracking (d)	120	90	>230	>220	180
Total shrinkage at 120 d (μm/m)	420	470	525	470	400

$7 \times 7 \times 28$ cm specimens was regularly measured in order to determine the loss of mass due to drying.

2.3.4. Restrained shrinkage tests

The ring tests [6,7] are used to evaluate the risk of cracking due to restrained shrinkage, by measuring an age of cracking. As shown in Fig. 1, the shrinkage of the concrete ring is hindered by the steel ring. By measuring the strain of the steel ring with the help of four strain gauges, it is possible to calculate the maximal tensile stress in the concrete ring, as detailed in [6]. A 20 mm notch is placed on the inner circumference of the steel ring in order to decrease

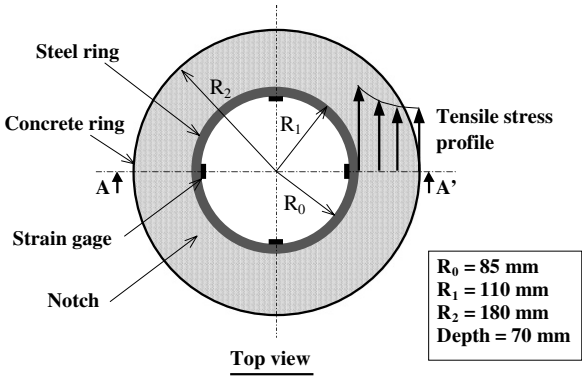

Fig. 1. Restrained shrinkage test or ring test.

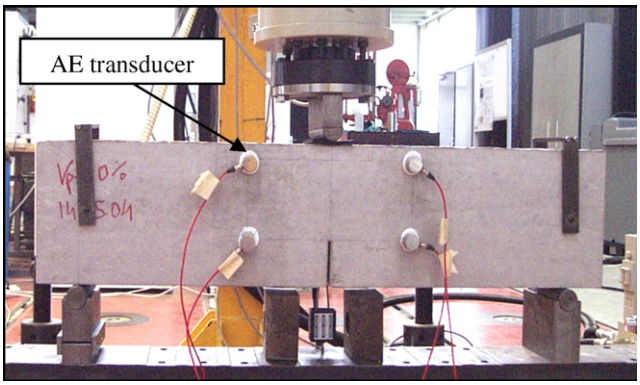

Fig. 3. AE transducers placement – rectangular array of 200×85 mm^2.

the test duration. The outer circumference of the concrete ring is covered by an aluminium foil: only the top and bottom surface can dry at 20 ± 2 °C and $50 \pm 5\%$ RH. The cross section of the concrete ring is the same as the $7 \times 7 \times 28$ cm specimen of the non-restrained shrinkage test.

2.3.5. Fracture properties

The concrete fracture was studied by carrying three points bending tests on nine notched beams. The dimensions of the beams were $100 \times 150 \times 700$ mm^3 [8]. The notch was 50 mm high and 2 mm wide. The tests were crack opening controlled with a rate of 0.05 μm/s. Crack mouth opening displacement (CMOD) was measured thanks to a sensor placed between two steel plates stuck on each side of the notch on the bottom face of the specimen. The test configuration is shown in Fig. 2.

The bending tests were performed on three mixtures of the first series: $V_p - 30\%$, $V_p - 10\%$ and $V_p + 30\%$. The fracture behavior is described through the two following approaches:

- Fracture behavior was first characterized by the fracture toughness G_F, i.e. the energy needed to produce a unit area of crack surface. It is assessed in this work from the area under the load deflection curve divided by the ligament area, in agreement with [9] for notched prismatic specimens under three-point bending.

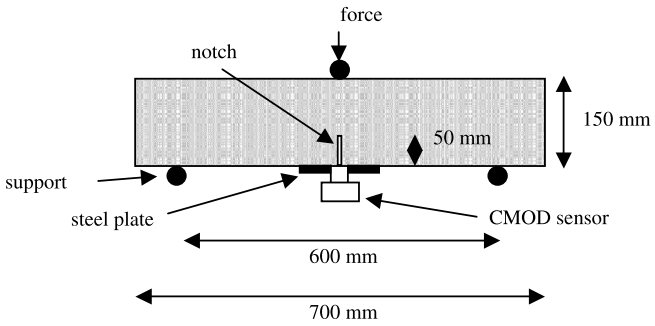

Fig. 2. Three points bending tests configuration.

- Fracture behavior was also characterized with the parameters from the two parameter fracture model (TPFM), i.e. the critical stress intensity factor K_{ic} and the critical crack tip displacement $CTOD_c$. These material parameters are deduced from initial compliance at peak load using the procedure in [10].

The fracture behavior of the specimens was also studied by acoustic emission (AE) tests. The technique has been first developed to monitor and inspect metallic structures. Then it was applied to concrete structures and now AE source location may be used to investigate the properties of the fracture process zone (FPZ) of concrete [11–13]. In order to follow and to characterize the cracking processes, three specimens made of the three mixtures were instrumented with four piezoelectric transducers (with a resonance frequency of 150 kHz). They formed a rectangular array of 200×85 mm^2 on one side of the specimens (Fig. 3), just above the notch, in order to cover the expected zone of the FPZ and to minimize the errors in the AE event location algorithms.

The transducers were coupled to the material with a silicon glue. The signal detection value (in amplitude) was set to 35 dB in order to overcome the background noise, and the detected signals were amplified with 40 dB gain amplifiers. A planar algorithm, from the commercial software AEWin [14], was used for AE location. 2D location maps of the micro-cracks detected are thus achieved, where all the events detected in the thickness of the specimen are projected onto the same place in the maps. The statistical error of location is about ±5 mm, which is calculated from conventional Hsu Nielsen simulations (used in [15]). The procedure is accurate if we consider the transducers diameter (15 mm) and the natural heterogeneity of the material (maximum aggregate size of 8 mm).

3. Results and discussion

3.1. Mechanical properties

In Fig. 4, the 28-day compressive strength of the Series 1 mixtures is shown to decrease with an increase in volume of

paste. Note that the dot of the reference mixture, circled on the figure, is in common for the three series. While the volume of paste increased by 57%, from 291 l to 457 l, the 28-day compressive strength only decreased by 12%, from 47.1 to 41.7 MPa.

This trend could be deduced neither from the W_{eff}/C ratio, which is kept constant in Series 1, nor from the variation of air content (roughly estimated at fresh state), which increased when the volume of paste decreased. Nevertheless, this trend has already been noticed in the case of vibrated concrete mixtures [16–19]. It has been modeled by de Larrard through the maximum thickness of paste (MPT) concept [17]. The author shows that the compressive strength of a concrete mixture decreases with an increase in MPT, i.e. the maximal interval between two consecutive gravels. The MPT increases with the volume of paste.

The opposite trend was reported by Amparano et al. [20], in a study dealing with concrete mixtures made of volumes of paste in the same range (from 25% to 55%) and about the same W/C ratio (0.50). In both studies the decrease or increase in strength is about 10% of the higher strength, which is relatively low. The two trends could be consistent and result from the same opposite effects. As it has been assumed in both analyses, aggregates are generally stronger than paste, for W/C ratios exceeding 0.5. So increasing aggregates content is likely to enhance strength of concrete. But aggregates are surrounded by interface transition zones (ITZ) that are more porous than the homogenous matrix [21]. So increasing aggregates volume increases volume and connectivity of ITZ and weakens concrete. The combination of these two opposite effects could result in a slight increase or decrease in strength. The differences may come from raw materials, composition parameters, such as the volume ratio of coarse to fine aggregates, and workability, which may be kept constant or not.

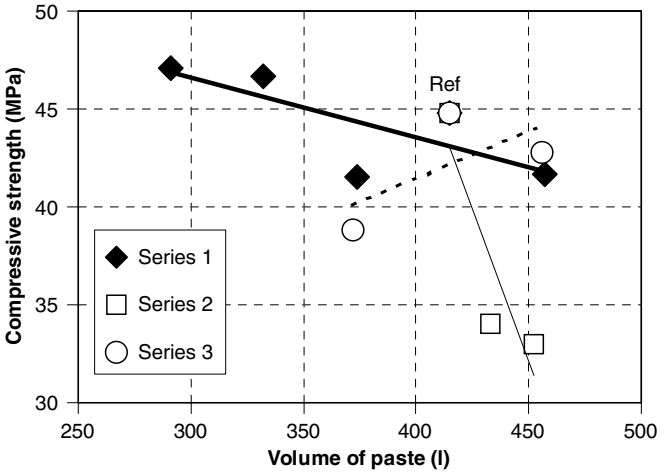

Fig. 4. Compressive strength at 28 days vs. volume of paste. Tendency lines are plotted: bold line (Series 1), fine line (Series 2) and dotted line (Series 3).

As expected, the compressive strength of Series 2 mixtures decreases clearly with an increase in water content (Fig. 4). This results mainly come from the increase in W_{eff}/C ratio (Table 3), since cement content is kept constant and water content increases.

As shown in Fig. 4, the evolution of compressive strength vs. the volume of paste is not linear when aggregates are replaced by limestone filler. This may be due to opposite effects of parameters, such as volume of paste, packing density and limestone chemical activity. Nevertheless, the global tendency is an increase of strength with higher limestone content, probably due to the limestone activity. The increase in limestone content could also improve the bond between aggregates and paste in the ITZ [21].

As seen in Fig. 5, the elastic modulus of the Series 1 mixtures decreased with an increase in volume of paste. This can be explained by the assumption that aggregates are generally stiffer than paste. As aggregates content decreases with an increase in volume of paste, the elastic modulus should also decrease.

In the case of the Series 2 and 3 mixtures, the effects of the mix-proportions changes on elastic modulus are less pronounced than those on compressive strength (Fig. 5). Anyway, the decrease in elastic modulus of Series 2 mixtures should be associated with the decrease in aggregates content and the reduction in paste stiffness with W_{eff}/C ratio. As suggested previously, the change in limestone content in Series 3 may have contrary effects, namely: on the one hand, the elastic modulus should decrease with lower aggregates content; on the other hand, the elastic modulus of paste could increase with higher limestone content and lower $W_{eff}/(C + LF)$ ratio.

3.2. Free shrinkage

In Figs. 6–8, total shrinkage and autogenous shrinkage are plotted against time. Extrapolation curves are also plotted to assess shrinkage strains at 400 days.

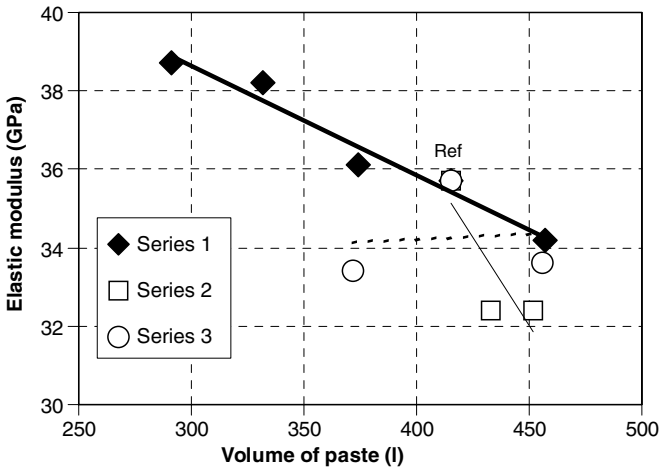

Fig. 5. Elastic modulus at 28 days vs. volume of paste. Tendency lines are plotted: bold line (Series 1), fine line (Series 2) and dotted line (Series 3).

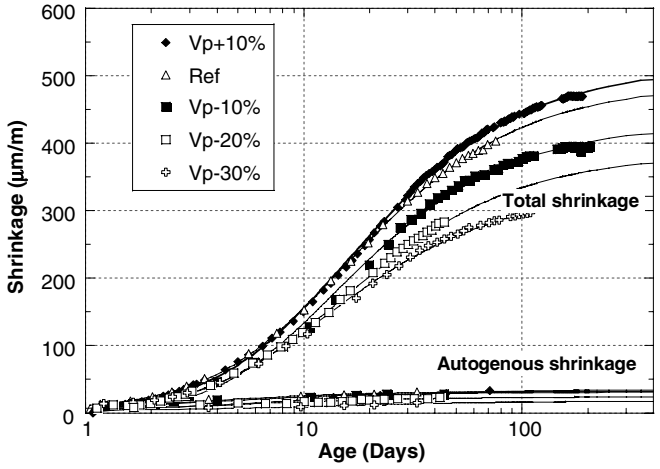

Fig. 6. Total shrinkage and autogenous shrinkage of the Series 1 mixtures.

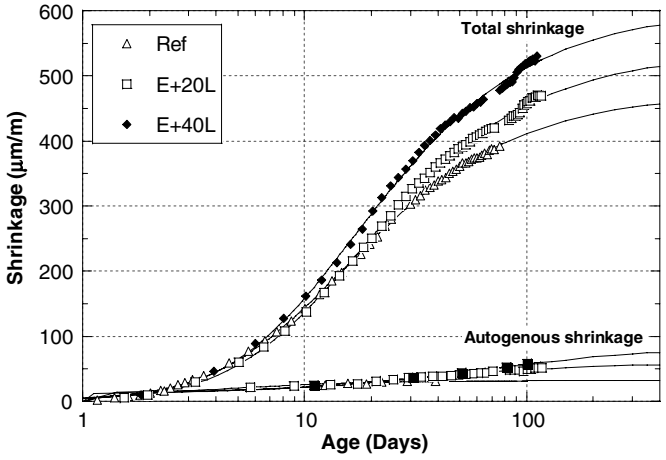

Fig. 7. Total shrinkage and autogenous shrinkage of the Series 2 mixtures.

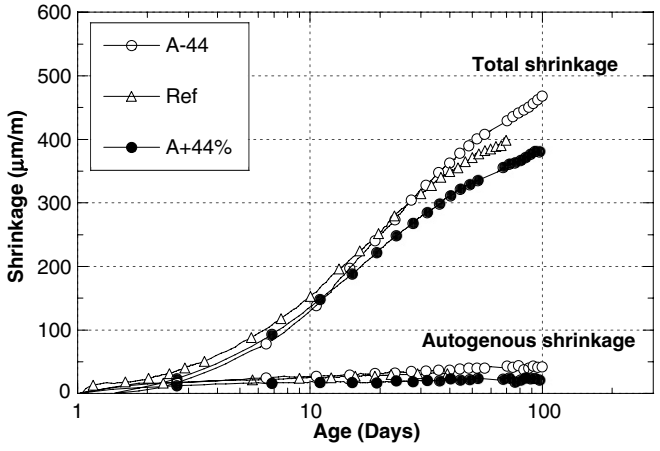

Fig. 8. Total shrinkage and autogenous shrinkage of the Series 3 mixtures.

The total shrinkage of our mixtures is mainly due to drying, because autogenous shrinkage is very low: less than 60 µm/m at 120 days. This is due to the relatively high tested W_{eff}/C ratios ($W_{eff}/C > 0.5$).

From Series 1 measurements, it can be deduced that shrinkage increased with an increase in the volume of paste. This result was expected since only paste shrinks due to drying. The drying kinetic, assessed through loss of mass measurements, tends also to increase with the volume of paste (Figs. 9–11). Note that the loss of mass was expressed in g per unit of sample length in order to permit a comparison with the shrinkage values expressed in µm/m, as explained hereafter. In the tested range of volumes of paste, the shrinkage amplitude at a given time increases almost linearly with the volume of paste (Fig. 12). This means that any reduction in volume of paste (ΔV_p) results in a decrease in shrinkage amplitude ($\Delta\varepsilon_s$), which can be roughly calculated by a linear relation: $\Delta\varepsilon_s = \alpha\Delta V_p$. Of course, the coefficient α depends on both the concrete age and the properties of the materials, such as the stiffness of aggregates [3,16].

This relation should also depend on specimen size. In fact, one should keep in mind that the measured shrinkage

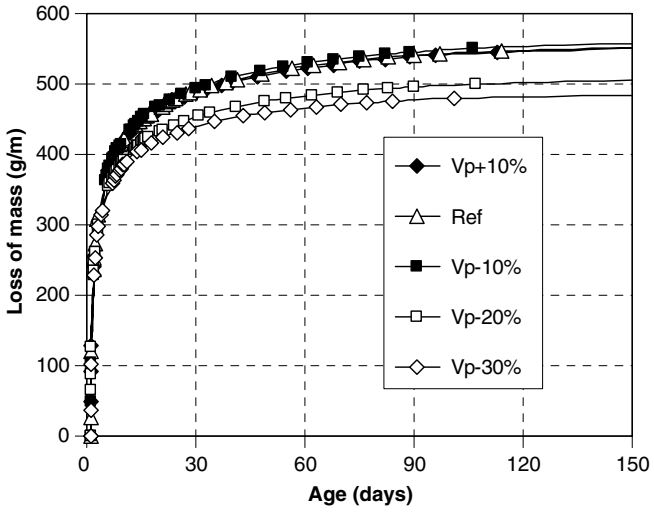

Fig. 9. Loss of mass of the Series 1 mixtures.

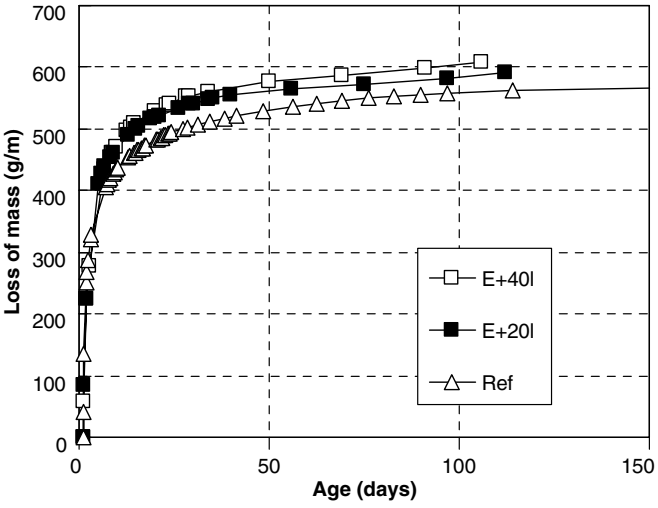

Fig. 10. Loss of mass of the Series 2 mixtures.

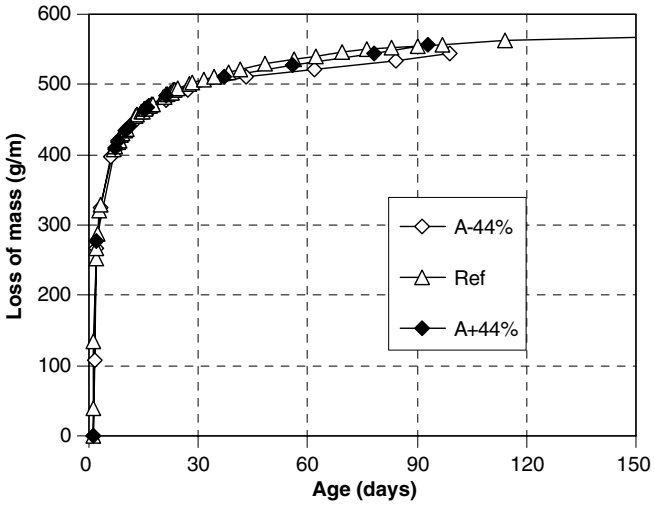

Fig. 11. Loss of mass of the Series 3 mixtures.

is not an intrinsic property, because the moisture gradient between the drying surface and the core of the specimen results inevitably in cracking of the concrete skin [22]. This phenomenon can be highlighted in Figs. 13–15. A calculated drying shrinkage, i.e. total shrinkage minus autogenous shrinkage, was plotted vs. the loss of mass, expressed in g/m. Two typical phases can be distinguished on these curves. During the first one, drying does not generate shrinkage. This is likely due to the cracking of the specimen skin. During the second phase, shrinkage increases almost linearly with drying degree. It is interesting to note that this second phase begins for the same loss of mass, whatever the volume of paste. This could mean that the skin cracking due to the moisture gradient is about similar, in the tested range of volumes of paste. Therefore, one can suppose that the measured changes in shrinkage amplitude result mainly from the changes in concrete composition, i.e. volume of paste, and not from this experimental drawback.

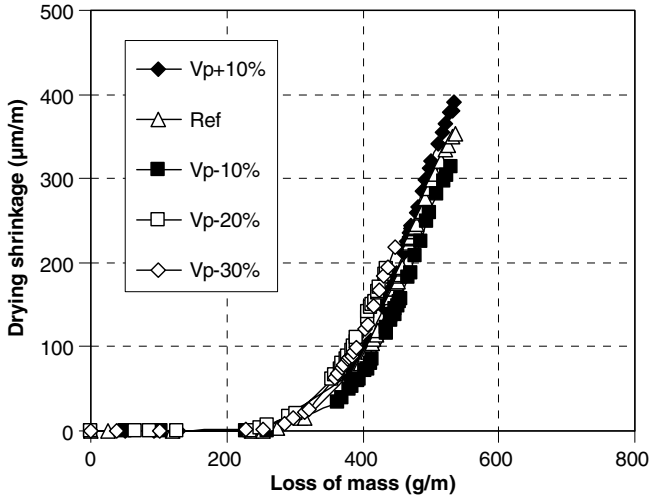

Fig. 12. Drying shrinkage vs. loss of mass of the Series 1 mixtures.

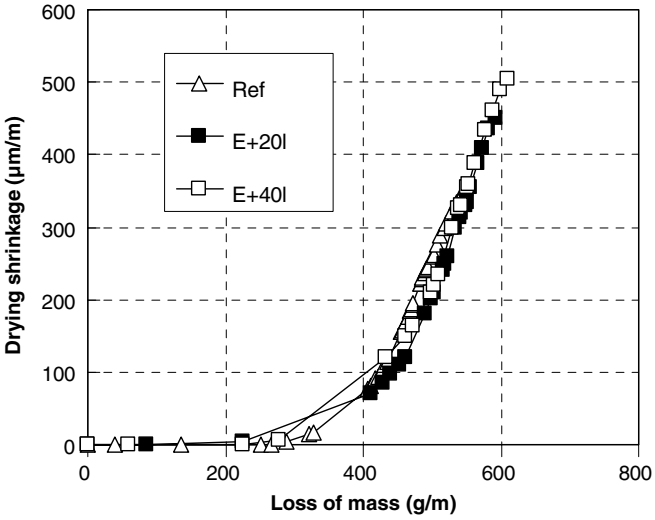

Fig. 13. Drying shrinkage vs. loss of mass of the Series 2 mixtures.

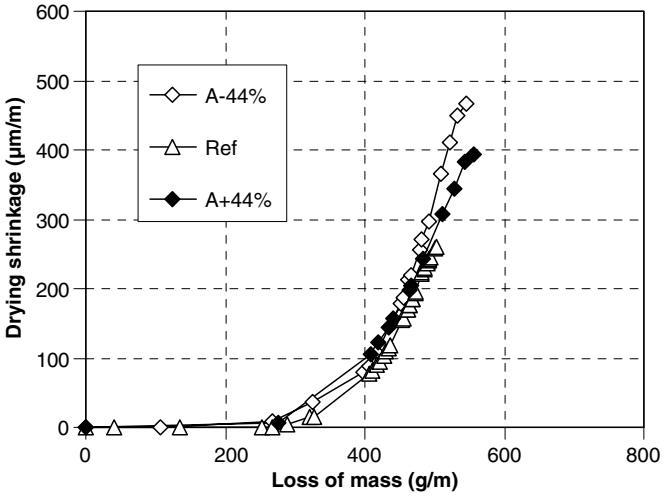

Fig. 14. Drying shrinkage vs. loss of mass of the Series 3 mixtures.

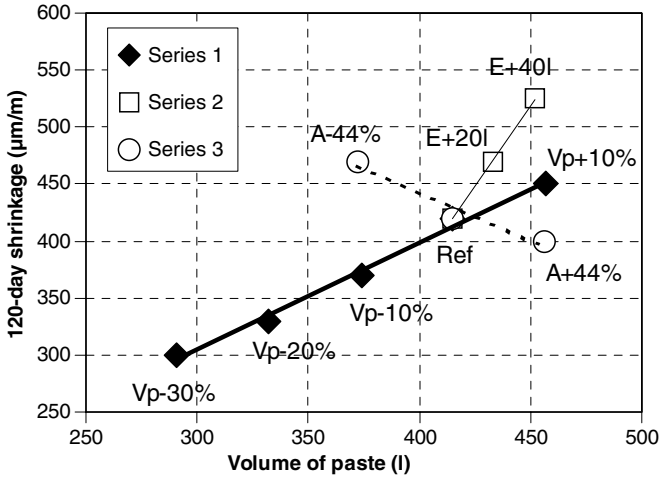

Fig. 15. Influence of volume of paste on 120-day shrinkage amplitude.

Shrinkage is proportional to the volume of paste, provided that the paste proportions, especially W_{eff}/C and LF/C, are constant (Series 1). If the volume of paste is increased by replacing aggregates by water, the increase in shrinkage, observed in Series 2, is much larger than in the case of Series 1 (Fig. 7). The increase in total shrinkage with water content is a consequence of the increase in open porosity and thus in drying kinetic, as shown in Fig. 10.

Conversely, the shrinkage amplitude was found to decrease when the volume of paste was increased by replacing aggregates by limestone filler, as measured in Series 3 (Fig. 8). However the drying kinetic remains however the same (Fig. 11). That means that differences in shrinkage would be caused by differences in the material properties, such as elastic modulus.

All the results on shrinkage are summed up in Fig. 15, with the example of 120-day shrinkage strain. The volume of paste has a noticeable effect on shrinkage, but the trend and the variation strongly depends on the paste proportions. It can be verified in Figs. 13 and 14 that the second phase of the shrinkage vs. drying curve begins almost for the same loss of mass. Thus, the skin cracking phenomenon is probably equivalent in Series 2 and 3. However, any generalization of these results should be done carefully, knowing that the size effect on drying was not investigated.

3.3. Shrinkage cracking

The evolution of tensile stress due to restrained shrinkage from the ring tests is shown in Figs. 16–18. It can be seen that the differences between the stress curves from the Series 1 are not as obvious as the differences between the shrinkage curves. In fact, the stress development does not only depend on shrinkage, but also on elastic modulus and creep. Any change in volume of paste results in changes in both shrinkage and visco-elastic properties. For instance, creep is known to increase with volume of paste [16]. Thus, changes in visco-elastic properties can reduce the effects of shrinkage. Nevertheless, the reduction in shrinkage with the volume of paste results in a decrease in stress level and in an increase of the age of cracking (Table 1): the reduction in volume of paste reduces the cracking risk.

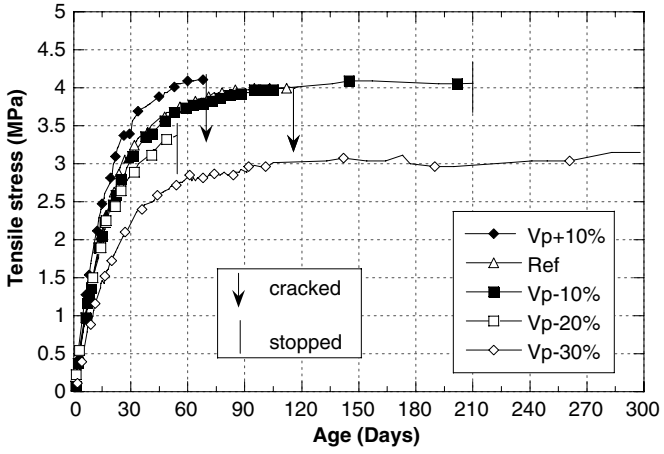

Fig. 16. Ring test of the Series 1 mixtures.

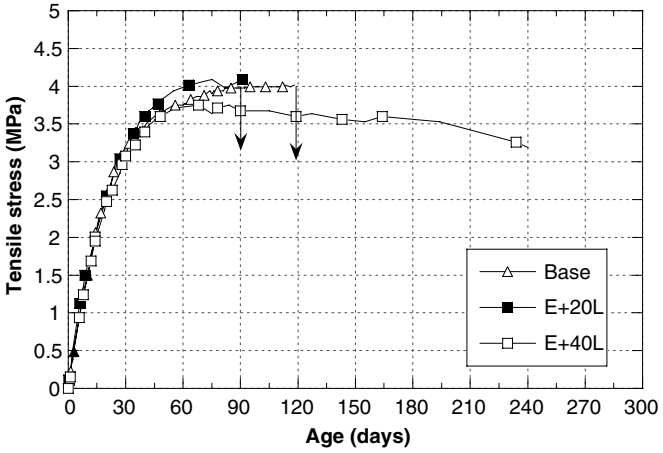

Fig. 17. Ring test of the Series 2 mixtures.

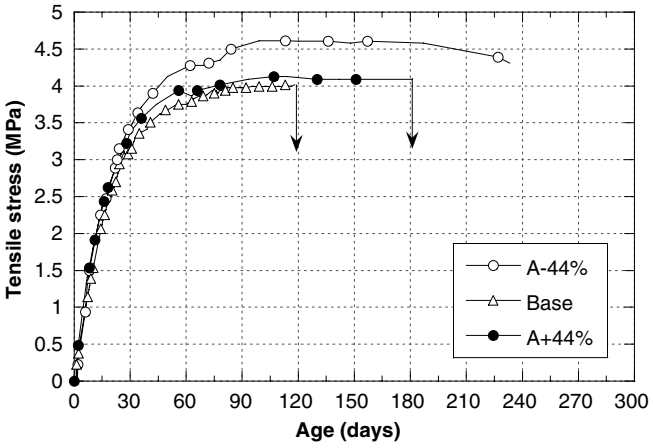

Fig. 18. Ring test of the Series 3 mixtures.

However, the good correlation between free shrinkage and age of cracking should be analyzed carefully. First, the boundary conditions of the shrinkage specimens and the rings are not quite equivalent. Indeed, the prismatic specimens can dry on their four lateral surfaces, while the rings can dry only on their two opposite surfaces and not on the circumferential surfaces covered by tap. The mean drying radius is not the same for the two kinds of specimen geometry. Secondly, as observed in Series 2 and 3, no direct correlation can be found between free shrinkage and restrained shrinkage. For instance, the stress development of the Series 2 mixtures is similar for the first two months, whereas their shrinkage is very different (Fig. 7). The Weff + 40 l mixture has the highest shrinkage values, but the concrete ring did not crack after 200 days and, moreover, the tensile stress decreased after 90 days. This stress relaxation is probably caused by creep. In Fig. 18, the LF − 44% mixture, did not crack, whereas it has the high-

est shrinkage. The results show that the stress development actually depends on shrinkage as well as visco-elastic properties.

3.4. Fracture properties

3.4.1. Fracture parameters and toughness

Fig. 19 shows the load vs. CMOD curves of three-point bending tests. The results reveal that there is no significant difference between the concrete mixtures. The effect of paste volume on K_{ic} and G_F is about the same as its effect on strength (Figs. 20 and 21). The effect on $CTOD_c$ is clearer: $CTOD_c$ increases with the volume of paste (Fig. 22). The variations of K_{ic} and $CTOD_c$ with the paste volume should result in variation of the fracture resistance of SCC, according to the TFPM model. However, it is difficult to say exactly how the volume of paste affects fracture resistance. Moreover, the effect on $CTOD_c$ could be the result of its effect on the elastic modulus.

The difference between these materials could be due to the width of FPZ which is formed ahead of the crack tip prior of the fracture. In this work, the FPZ width is characterized by acoustic emission (AE) technique.

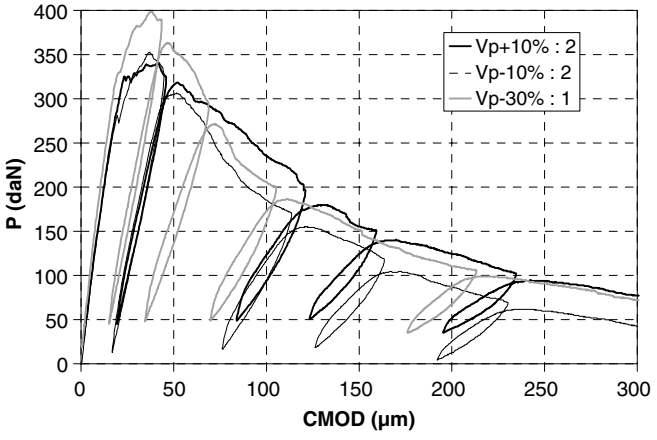

Fig. 19. Results of the bending tests: charge vs. CMOD.

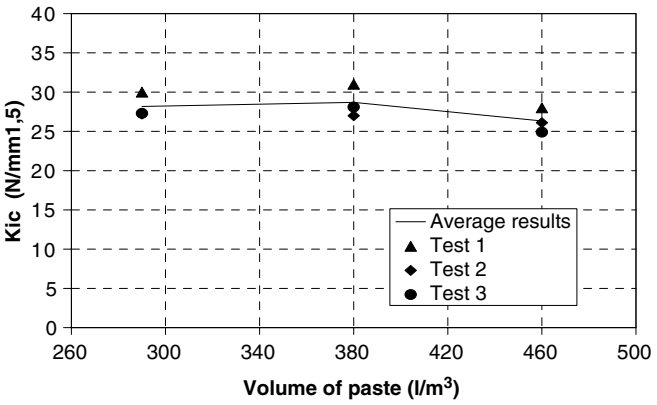

Fig. 20. K_{ic} vs. volume of paste.

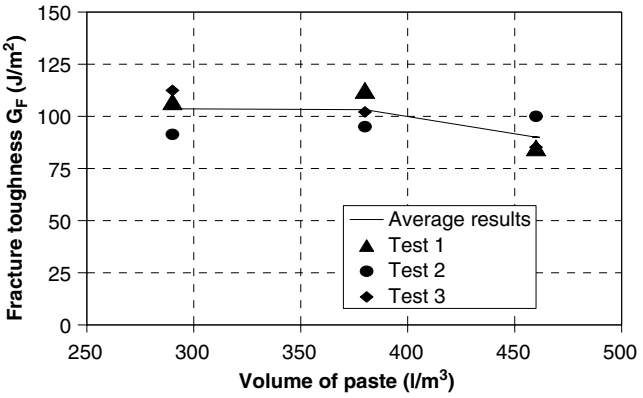

Fig. 21. G_F vs. volume of paste.

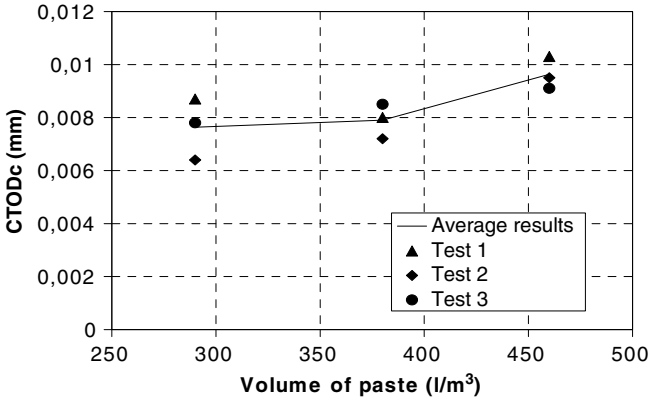

Fig. 22. $CTOD_c$ vs. volume of paste.

3.4.2. Estimation of FPZ width by acoustic emission

The aim of AE analysis was to get an experimental characterization of the FPZ, and more specifically of its width related to the internal length in continuum damage models. The locations maps of micro-cracks detected (called AE events) for a specimen made of $V_p - 30\%$ mixture and for a specimen made of $V_p + 10\%$ mixture are presented in Fig. 23. The maps are obtained after selecting the signals with amplitude less than 50 dB, in order to keep only the most energetic micro-cracks associated with concrete fracture [11]. The plotted points indicate the detected AE events.

On these maps, it can be seen that, for the $V_p - 30\%$ specimen, AE events were located into a larger area than for the $V_p + 10\%$ specimen. The approach adopted to estimate the crack band width associated with the FPZ consists in plotting the cumulative number of detected events as a function of the horizontal position. The number of events is measured in a horizontal band of 5 mm width (the width between two horizontal transducers is thus divided in zones of 5 mm). The measurement is performed at a stated reference COD, taken in this study at 450 µm, which corresponds approximately to the end of the bending test where the applied load is close to 0. Gaussian curves are thus obtained if the histogram got from the measure-

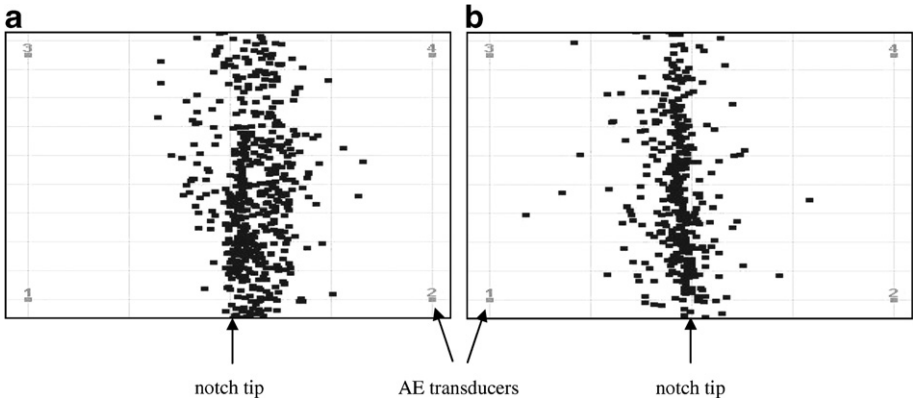

Fig. 23. Cumulative location maps of AE events: (a) $V_p - 30\%$ mixture; (b) $V_p + 10\%$ mixture.

ments is smoothed. Fig. 24 represents the average smoothed curves for the three specimens of each mixture.

In order to compare the FPZ sizes for the three different volumes of paste, an horizontal line, which intersects the y-axis (number of events), at 10% and 25% of the maximum number of events detected, can be plotted on the same graph as shown in Fig. 25. We define arbitrarily the crack band width as the length of the segment of the horizontal straight line which intersects the distribution of AE events [13]. By this way, a comparison of the FPZ width estimations (relative to the defined percentage) is possible for the three mixtures.

At 10% of the maximum number of events, the average estimation of the FPZ width are 43.6, 40.3 and 37.8 mm for $V_p - 30\%$, $V_p - 10\%$ and $V_p + 10\%$ mixtures, respectively. At 25%, the values are respectively 25.7, 22.7 and 19 mm.

The results show a significant decrease of the width of the FPZ with an increase of the volume of paste, and the trend was the same for the 2% chosen for the analysis. This decrease of the FPZ width can be explained by the fact that crack propagation in concrete is strongly influenced by any inclusions (aggregates for instance) in the matrix (paste). Indeed, micro-cracks develop in the matrix and join in order to form the macro-crack. Using acoustic emission, Chen and Liu [23,24] have thus shown the decrease of the FPZ width with the increase of maximum aggregates size (which varied from 5 mm to 20 mm). The work of Otsuka and Date [11] also provides the same results by the investigation of the FPZ by both acoustic emission and X-ray technique. In the present study, the maximum aggregates size was constant and the average size decreased with an increase in paste volume. We can thus make an analogy with the cited works and postulate that the decrease of the FPZ width would be the consequence of the decrease of the average aggregates size when the paste volume increases.

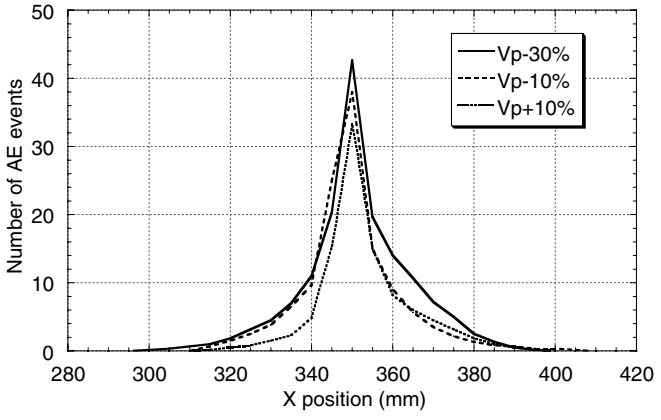

Fig. 24. Evolution of cumulative detected events as a function of horizontal position in the location array ($X = 350$ mm corresponds to the notch).

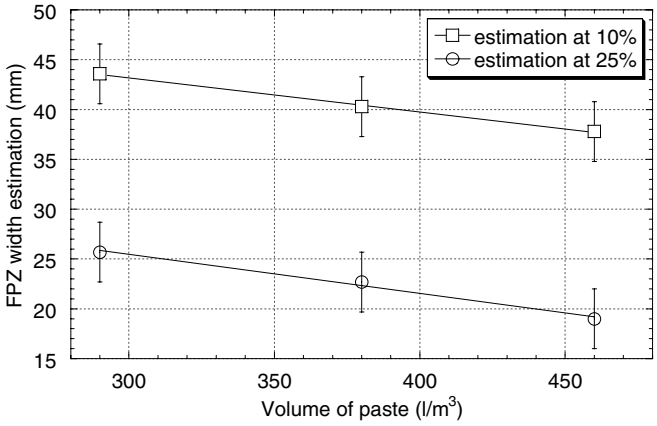

Fig. 25. Evolution of the FPZ estimation for the three mixtures, at 10% and 25% of the maximum of AE events detected.

4. Conclusions

The experimental results reported and discussed in this paper concern three major composition parameters of self-compacting concrete mixtures, namely: volume of paste, water content, and mineral admixtures content. A first series of concrete mixtures was designed varying the volume of paste and keeping the proportions of its constituents (cement, water, mineral and chemical admixtures) constant. From a reference mixture of the first series, the

volume of paste of the second and third series of concrete mixtures was increased or decreased only by changing the water content (Series 2) and mineral admixture content (Series 3). Strength, modulus, shrinkage, shrinkage cracking properties and fracture behavior were assessed and the following conclusions have been drawn:

- The volume of paste had a restricted effect on strength and elastic modulus. The slight decrease of these properties with an increase in the volume of paste could be due to opposites effects of the aggregates on the internal structure of concrete and on the interface transition zones in cementitious matrix. These effects could also account for the slight decrease of the fracture process zone width and fracture toughness. Non-restrained shrinkage was shown to increase almost linearly with an increase in volume of paste, but these results do not account for restrained shrinkage behavior assessed through the ring test, because that also depends on the visco-elastic properties of concrete. However, increasing the volume of paste increases shrinkage cracking susceptibility.
- As expected, an increase in water content caused a drop in strength and modulus. The increase in shrinkage and shrinkage cracking susceptibility was more pronounced than that was observed for the same variation of paste volume in the first series. This was mainly due to drying shrinkage, as the W_{eff}/C (effective water/cement) ratio was rather high (more than 0.54) and autogenous shrinkage remained very low.
- Changing the mineral admixture content did not affect significantly strength and mechanical properties, in the studied range. Increasing the mineral admixture content reduced non-restrained shrinkage but it seemed to increase the risk of cracking.

This study was done to gain insight into practical ways to optimize the formulation of SCC. Reducing the volume of paste may affect flowability and facing quality, but it is a way to reduce shrinkage and risk of cracking without affecting much strength. Another way to optimize SCC mixtures is to work on composition parameters of the paste, such as mineral admixture type and content. Ongoing study on this issue is to give complementary results. However, these are not all intrinsic properties, but rather some depend on the testing devices and procedures. Therefore designers have to choose relevant tests and properties to take into account the actual exposure conditions.

References

[1] Walraven J. Structural aspects of self-compacting concrete. In: Wallevik O, Nielsson I, editors. Proceedings of third RILEM international symposium on self-compacting concrete. Reykjavik, Iceland: RILEM Publications; 2003.
[2] Hammer TA. Cracking susceptibility due to volume changes of self-compacting concrete. In: Wallevik O, Nielsson I, editors. Proceedings of third RILEM international symposium on self-compacting concrete. Reykjavik, Iceland: RILEM Publications; 2003.
[3] Bissonnette B, Pierre P, Pigeon M. Influence of key parameters on drying shrinkage of cementitious materials. Cem Concr Res 1999;25(5):1075–85.
[4] French Association of Civil Engineering. Self-compacting concrete, Interim recommendations. AFGC, 2002.
[5] Spinner E, Teft WE. A method for determining mechanical resonance frequencies and for calculating elastic modulus from these frequencies. In: Proceedings of the ASTM, 1961.
[6] Turcry P. Retrait et fissuration des bétons autoplaçants – Influence de la formulation. PhD Thesis, Nantes, Ecole Centrale de Nantes, 2004 [in French].
[7] Hossain AB, Weiss WJ. Assessing residual stress development and stress relaxation in restrained concrete ring specimens. Cem Concr Compos 2004;26(5):531–40.
[8] Rozière E, Turcry P, Loukili A, Granger S. Influence of paste volume of fracture behavior of self-compacting concrete. In: Pijaudier-Cabot G, Gérard B, Acker P, editors. Proceedings of the 7th international conference concreep7. Nantes, France: Lavoisier Publications; 2005.
[9] RILEM. Determination of the fracture of mortar and concrete by means of three-point tests on notched beam. Mater Struct 1985;18(4):291–6.
[10] Jansen DC, Weiss WJ, Schleuchardt SHF. Modified testing procedure for the two parameter fracture model for concrete. In: Proceedings of the 13th ASCE engineering mechanics conference, New York, 2000.
[11] Otsuka K, Date H. Fracture process zone in concrete tension specimen. Eng Fract Mech 2000;65(2–3):111–31.
[12] Mihashi H, Nomura N. Correlation between characteristics of fracture process zone and tension-softening properties of concrete. Nucl Eng Des 1996;165(3):359–76.
[13] Haidar K, Pijaudier-Cabot G, Dubé JF, Loukili A. Correlation between the internal length, the fracture process zone and size effect in model materials. Mater Struct 2005;38:201–10.
[14] Proust A, Marlot D, Lenain JC. Application of acoustic emission to detect damage in concrete structures, illustrated with full scale examples. In: Proceedings of concrete solutions, 1st international conference on concrete repair, Saint Malo, France, 2003.
[15] Granger S, Loukili A, Pijaudier-Cabot G, Chanvillard G. Experimental characterization of the self healing of cracks in an ultra high performance cementitious material: mechanical tests and acoustic emission analysis. Cem Concr Res 2007;37(4):519–27.
[16] Neville AM. Properties of concrete. Eyrolles Editions; 2000.
[17] De Larrard F. Concrete mixture-proportioning. E&FN Spon; 1999.
[18] Stock AF, Hannant DJ, Williams RIT. The effect of aggregate concentration upon the strength and modulus of elasticity of concrete. Mag Concr Res 1979;31(109):225–34.
[19] Kolias S, Georgiou C. The effect of paste volume and of water content on the strength and water absorption of concrete. Cem Concr Compos 2005;27(2):211–6.
[20] Amparano FE, Xi YP, Roh YS. Experimental study on the effect of aggregate content on fracture behavior of concrete. Eng Fract Mech 2000;67(1):65–84.
[21] Ollivier JP, Maso JC, Bourdette B. Interfacial transition zone in concrete. Adv Cem Based Mater 1995;2(1):30–8.
[22] Benboudjema F, Meftah F, Torrenti JM. Interaction between drying, shrinkage, creep and cracking phenomena in concrete. Eng Struct 2005;27(2):239–50.
[23] Chen B, Liu J. Effect of aggregate on the fracture behavior of high strength concrete. Constr Build Mater 2004;18(8):585–90.
[24] Chen B, Liu J. Investigation of effects of aggregate size on the fracture behavior of high performance concrete by acoustic emission. Constr Build Mater 2006;21(8):1696–701.